Thermodynamic controls on rates of iron oxide reduction by extracellular electron shuttles

Meret Aeppli[a,b,1], Sébastien Giroud[a], Sanja Vranic[a], Andreas Voegelin[b], Thomas B. Hofstetter[a,b,2], and Michael Sander[a,2]

[a]Institute of Biogeochemistry and Pollutant Dynamics, ETH Zürich, 8092 Zürich, Switzerland; and [b]Eawag, Swiss Federal Institute of Aquatic Science and Technology, 8600 Dübendorf, Switzerland

Edited by Dianne Newman, Division of Biology and Biological Engineering and the Division of Geological and Planetary Sciences, California Institute of Technology, Pasadena, CA; received August 24, 2021; accepted November 19, 2021

Anaerobic microbial respiration in suboxic and anoxic environments often involves particulate ferric iron (oxyhydr-)oxides as terminal electron acceptors. To ensure efficient respiration, a widespread strategy among iron-reducing microorganisms is the use of extracellular electron shuttles (EES) that transfer two electrons from the microbial cell to the iron oxide surface. Yet, a fundamental understanding of how EES–oxide redox thermodynamics affect rates of iron oxide reduction remains elusive. Attempts to rationalize these rates for different EES, solution pH, and iron oxides on the basis of the underlying reaction free energy of the two-electron transfer were unsuccessful. Here, we demonstrate that broadly varying reduction rates determined in this work for different iron oxides and EES at varying solution chemistry as well as previously published data can be reconciled when these rates are instead related to the free energy of the less exergonic (or even endergonic) first of the two electron transfers from the fully, two-electron reduced EES to ferric iron oxide. We show how free energy relationships aid in identifying controls on microbial iron oxide reduction by EES, thereby advancing a more fundamental understanding of anaerobic respiration using iron oxides.

microbial iron oxide reduction | anaerobic respiration | free energy relationship | one-electron reduction potential

The use of iron oxides as terminal electron acceptors in anaerobic microbial respiration is central to biogeochemical element cycling and pollutant transformations in many suboxic and anoxic environments (1–6). To ensure efficient electron transfer to solid-phase ferric iron, Fe(III), at circumneutral pH, metal-reducing microorganisms from diverse phylae use dissolved extracellular electron shuttle (EES), including quinones (7–9), flavins (10–16), and phenazines (17–19), to transfer two electrons per EES molecule from the respiratory chain proteins in the outer membrane of the microbial cell to the iron oxide (17, 20, 21). The oxidized EES can diffuse back to the cell surface for rereduction, thereby completing the catalytic redox cycle involving the EES.

The electron transfer from the reduced EES to Fe(III) is considered a key step in overall microbial Fe(III) respiration. Several lines of evidence suggest that the free energy of the electron transfer reaction, $\Delta_r G$, controls Fe(III) reduction rates (15, 17, 22, 23). For instance, microbial Fe(III) oxide reduction by dissolved model quinones as EES was accelerated only for quinones with standard two-electron reduction potentials, $E^0_{H,1,2}$, that fell into a relatively narrow range of -180 ± 80 mV at pH 7 (24). Furthermore, in abiotic experiments, Fe(III) reduction rates by EES decreased with increasing $\Delta_r G$ that resulted from increasing either $E^0_{H,1,2}$ of the EES (25, 26), the concentration of Fe(II) in the system (27), or solution pH (25, 26, 28). However, substantial efforts to relate Fe(III) reduction rates for different EES species, iron oxides, and pH to the $E^0_{H,1,2}$ averaged over both electrons transferred from the EES to the iron oxides were only partially successful (25, 28). Reaction free energies of complex redox processes involving the transfer of multiple electrons can readily be calculated using differences in the reduction potentials averaged over all electrons transferred, and this approach is well established in biogeochemistry and microbial ecology. For kinetic considerations, however, the use of averaged reduction potentials is inappropriate.

Herein, we posit that rates of Fe(III) reduction by EES instead relate to the $\Delta_r G$ of the less exergonic first one-electron transfer from the two-electron reduced EES species to the iron oxide, following the general notion that reaction rates scale with reaction free energies (29). Our hypothesis is based on the fact that, at circumneutral to acidic pH and for many EES, the reduction potential of the first electron transferred to the fully oxidized EES to form the one-electron reduced intermediate semiquinone species, $E_{H,1}$, is lower than the reduction potential of the second electron transferred to the semiquinone to form the fully two-electron reduced EES species, $E_{H,2}$ [i.e., $E_{H,1} < E_{H,2}$ (30–33)]. This difference in one-electron reduction potentials implies that the two-electron reduced EES (i.e., the hydroquinone) is the weaker one-electron reductant for Fe(III) as compared to the semiquinone species. We therefore expect that rates of iron oxide reduction relate to the $\Delta_r G$ of the first electron transferred

Significance

Under anoxic conditions, various microorganisms couple the oxidation of organic carbon to the reduction of solid ferric iron oxide phases using extracellular electron shuttles (EES). Determining the contribution of this widespread terminal electron accepting process to total anaerobic respiration has proven challenging because of large variations in observed ferric iron reduction rates. This study demonstrates that rates of ferric iron oxide reduction by EES can be rationalized based on a unifying relationship that links rates to the thermodynamic driving force for the least favorable electron transfer from the EES to ferric iron. The relationship derived herein allows for a generalized and precise assessment of the contribution of EES-facilitated ferric iron oxide reduction to organic matter decomposition in anoxic environments.

Author contributions: M.A., T.B.H., and M.S. designed research; M.A., S.G., and S.V. performed research; M.A., S.G., and S.V. analyzed data; and M.A., A.V., T.B.H., and M.S. wrote the paper.

The authors declare no competing interest.

This article is a PNAS Direct Submission.

[1]Present address: Department of Earth System Science, Stanford University, Stanford, CA 94305.

[2]To whom correspondence may be addressed. Email: thomas.hofstetter@eawag.ch or michael.sander@env.ethz.ch.

This article contains supporting information online at https://www.pnas.org/lookup/suppl/doi:10.1073/pnas.2115629119/-/DCSupplemental.

Published January 11, 2022.

from the hydroquinone to Fe(III). The $\Delta_r G$ of this first electron transfer may even be endergonic provided that the two-electron transfer is exergonic.

We verified our hypothesis in abiotic model systems by demonstrating that reduction rates of two geochemically important crystalline iron oxides, goethite and hematite, by two-electron reduced quinone- and flavin-based EES over a wide pH range, and therefore thermodynamic driving force for Fe(III) reduction, correlate with the $\Delta_r G$ of the first electron transferred from the fully reduced EES to Fe(III). We further show that rates of goethite and hematite reduction by EES reported in the literature are in excellent agreement with our rate data when comparing rates on the basis of the thermodynamics of the less exergonic first of the two electron transfers.

Results and Discussion

Free Energies of Fe(III) Reduction by EES. We illustrate the differences of reaction free energies for the reduction of Fe(III) oxides by the first vs. second electron transferred from EES for two widely used EES, anthraquinone-2,6-disulfonate (AQDS) and riboflavin. Fig. 1*A* shows the E_H–pH diagram for AQDS with colored lines depicting the reduction potentials, $E^{0'}_{H,x}$, for the half-reactions specified in Eqs. **1**–**3** at pH 4 to 8. The reduction potential of the first electron transferred to $AQDS^{2-}$ to form the semiquinone radical anion species $AQDS^{\bullet 3-}$, $E^{0'}_{H,1}$ (Eq. **1**; orange line in Fig. 1*A*) is low and pH-independent given that the formed semiquinone is deprotonated over the environmentally relevant pH range considered here [i.e., $pK_a^{AQDSH^{\bullet 2-}} = 3.0$ (31); *SI Appendix*, Fig. S1]. By comparison, the reduction potential of the second electron transferred to the semiquinone, $E^{0'}_{H,2}$, is higher and has a slope of $-0.118\ V \cdot pH^{-1}$, resulting from the stoichiometric transfer of two protons with this electron (Eq. **2**; blue line in Fig. 1*A*). Under these conditions, the thermodynamics of the single-electron transfer steps result in only very small concentrations of the transient semiquinone species. The reduction potential for the transfer of both electrons, $E^{0'}_{H,1,2}$, is the average of $E^{0'}_{H,1}$ and $E^{0'}_{H,2}$ and has a slope of $-0.059\ V \cdot pH^{-1}$ (Eq. **3**; red line in Fig. 1*A*).

$$AQDS^{2-} + e^- \rightleftharpoons AQDS^{\bullet 3-} \quad [1]$$

$$AQDS^{\bullet 3-} + e^- + 2H^+ \rightleftharpoons AQDSH_2^{2-} \quad [2]$$

$$AQDS^{2-} + 2e^- + 2H^+ \rightleftharpoons AQDSH_2^{2-} \quad [3]$$

Fig. 1*A* also shows the reduction potential of the goethite (α-FeOOH)/Fe^{2+} redox couple with a slope of $-0.177\ V \cdot pH^{-1}$, reflecting the transfer of three protons per electron according to Eq. **4**.

$$\alpha\text{-FeOOH} + e^- + 3H^+ \rightleftharpoons Fe^{2+} + 2H_2O. \quad [4]$$

The resulting complete redox reactions for both the single-electron transfers (Eqs. **5** and **6** for the first and second electron

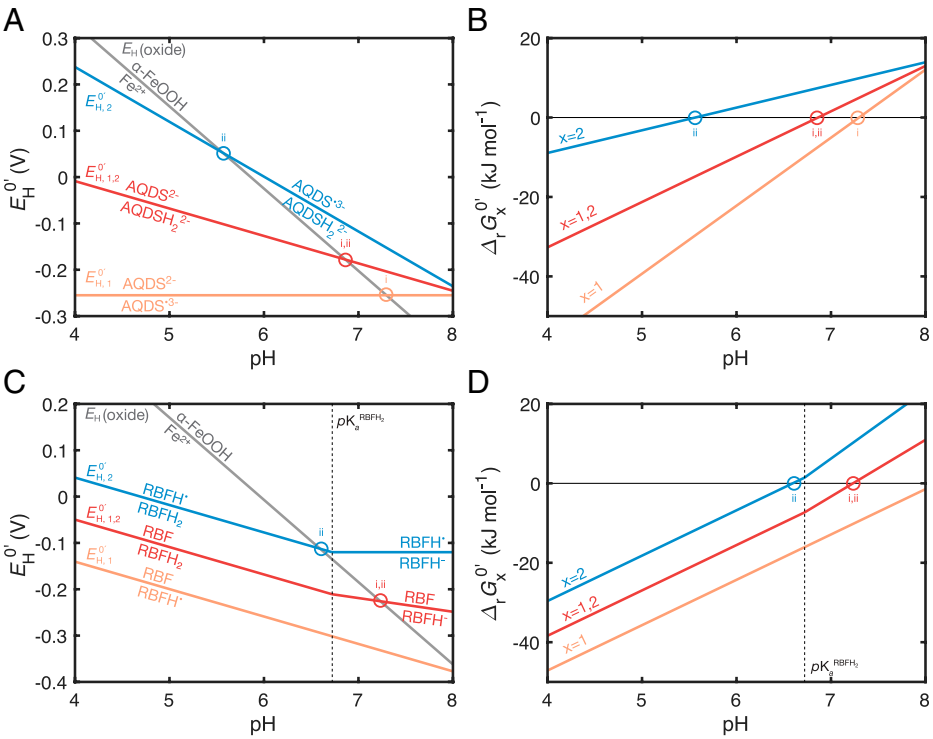

Fig. 1. Thermodynamic analysis of the reduction of goethite (α-FeOOH) by AQDS and riboflavin over the pH range examined in this work. (*A* and *C*) Pourbaix diagrams for redox couples quinone/hydroquinone ($E^{0'}_{H,1,2}$, red), semiquinone/hydroquinone ($E^{0'}_{H,2}$, blue), and quinone/semiquinone ($E^{0'}_{H,1}$, orange) of AQDS and riboflavin. The redox couple α-FeOOH/Fe^{2+} (E_H(oxide)) is shown as a gray line. $E^{0'}_H$–pH diagrams were drawn using published standard reduction potentials [AQDS (31, 34), riboflavin (33, 35, 36), *SI Appendix*, Table S1 and 0.768 V (37) for α-FeOOH]. Molecular structures of redox-active species of AQDS and riboflavin are shown in *SI Appendix*, Figs. S1 and S2, respectively. (*B* and *D*) Free energies, $\Delta_r G^{0'}_x$, of the two-electron transfer from reduced AQDS and riboflavin (x = 1,2: red lines) to α-FeOOH, and of the individual one-electron transfers; x = 2 (blue lines) stands for the first one-electron transfer from the fully reduced hydroquinone to α-FeOOH; x = 1 (orange lines) for the second one-electron transfer from the semiquinone to α-FeOOH. $\Delta_r G^{0'}_x$ values were calculated from the difference in reduction potentials between the α-FeOOH/Fe^{2+} redox couple and the redox couples of AQDS and riboflavin in *A* and *C* according to Eq. **18** and as detailed in *Materials and Methods*. The conditions at which $\Delta_r G^{0'}_x = 0$ kJ · mol^{-1} are marked in *A*–*D* by circles (○) labeled "i,ii" for x = 1,2 (red), "ii" for x = 2 (blue), and "i" for x = 1 (orange). Vertical lines in *B* and *D* denote the pK_a of the reduced riboflavin species.

transferred, respectively) as well as average combined two-electron transfer (Eq. **7**) are

$$\alpha\text{-FeOOH} + \text{AQDSH}_2^{2-} + \text{H}^+ \rightleftharpoons \text{Fe}^{2+} + \text{AQDS}^{\bullet 3-} + 2\text{H}_2\text{O} \quad \textbf{[5]}$$

$$\alpha\text{-FeOOH} + \text{AQDS}^{\bullet 3-} + 3\text{H}^+ \rightleftharpoons \text{Fe}^{2+} + \text{AQDS}^{2-} + 2\text{H}_2\text{O} \quad \textbf{[6]}$$

$$2\alpha\text{-FeOOH} + \text{AQDSH}_2^{2-} + 4\text{H}^+ \rightleftharpoons 2\text{Fe}^{2+} + \text{AQDS}^{2-} + 4\text{H}_2\text{O}. \quad \textbf{[7]}$$

We calculated the Gibbs free energies, $\Delta_r G_x^{0'} = -nF \cdot \Delta E_{\text{H},x}^{0'}$ (in kilojoules per mole of transferred electrons), for α-FeOOH reduction by AQDSH_2^{2-} (Eqs. **5**–**7**) from the differences in reduction potentials at any given pH ($\Delta E_{\text{H},x}^{0'}$) between the α-FeOOH/Fe^{2+} redox couple and the semiquinone/hydroquinone, quinone/semiquinone, and quinone/hydroquinone redox couples of the EES as in Eqs. **8**–**10**.

$$\Delta E_{\text{H},2}^{0'} = E_{\text{H}}^0(\alpha\text{-FeOOH}) - 2.303\frac{RT}{F}\left(\log\{\text{Fe}_{\text{aq}}^{2+}\} + 3\ \text{pH}\right) - \left(E_{\text{H},2}^0 - 2.303\frac{RT}{F}\left(\log\frac{\{\text{AQDSH}_2^{2-}\}}{\{\text{AQDS}^{\bullet 3-}\}} + 2\ \text{pH}\right)\right) \quad \textbf{[8]}$$

$$\Delta E_{\text{H},1}^{0'} = E_{\text{H}}^0(\alpha\text{-FeOOH}) - 2.303\frac{RT}{F}\left(\log\{\text{Fe}_{\text{aq}}^{2+}\} + 3\ \text{pH}\right) - \left(E_{\text{H},1}^0 - 2.303\frac{RT}{F}\log\frac{\{\text{AQDS}^{\bullet 3-}\}}{\{\text{AQDS}^{2-}\}}\right) \quad \textbf{[9]}$$

$$\Delta E_{\text{H},1,2}^{0'} = E_{\text{H}}^0(\alpha\text{-FeOOH}) - 2.303\frac{RT}{F}\left(\log\{\text{Fe}_{\text{aq}}^{2+}\} + 3\ \text{pH}\right) - \left(E_{\text{H},1,2}^0 - 2.303\frac{RT}{2F}\left(\log\frac{\{\text{AQDSH}_2^{2-}\}}{\{\text{AQDS}^{2-}\}} + 2\ \text{pH}\right)\right). \quad \textbf{[10]}$$

In these equations, F is the Faraday constant, $E_{\text{H}}^0(\alpha\text{-FeOOH})$ is 0.768 V (37), R is the gas constant, T is the absolute temperature, $\{\text{Fe}_{\text{aq}}^{2+}\}$ is the activity of dissolved Fe^{2+}, and $E_{\text{H},x}^0$ is the standard reduction potential of the redox couples semiquinone/hydroquinone ($x = 2$; Eq. **8**), quinone/semiquinone ($x = 1$ Eq. **9**), and quinone/hydroquinone ($x = 1, 2$; Eq. **10**). Note that $E_{\text{H},x}^{0'}$ values were calculated using the experimental proton activity and assumed equal activities of the hydroquinone, quinone, and semiquinone species of the EES (hence the superscript $^{0'}$). This assumption was necessary because we could not experimentally quantify concentrations of semiquinones due to their transient nature.

Fig. 1*B* shows that $\Delta_r G_x^{0'}$ increases with increasing pH with slopes reflecting the proton stoichiometries in Eqs. **5**–**7**. More importantly, $\Delta_r G_2^{0'}$ is less negative than $\Delta_r G_1^{0'}$ over the entire pH range shown. Therefore, the transfer of the first electron from the hydroquinone to α-FeOOH is less exergonic (and even endergonic above pH 5.6) than the transfer of the second electron from the semiquinone to α-FeOOH. The difference in free energies of α-FeOOH reduction by the first and the second electron transferred from the EES increases with decreasing pH from 2 $\text{kJ} \cdot \text{mol}^{-1}$ at pH 8.0 to as much as 36 $\text{kJ} \cdot \text{mol}^{-1}$ at pH 5.0. We therefore expect that rates of α-FeOOH reduction by a fully reduced EES relate to the driving force of the first electron transferred from the ESS to Fe(III) on the basis of the general notion that rates of electron transfer reactions scale with reaction free energies in the normal Marcus region (29).

We conducted the same thermodynamic analysis for the reduction of α-FeOOH by riboflavin (Fig. 1 *C* and *D*, see species in *SI Appendix*, Fig. S2). Calculated $E_{\text{H},x}^{0'}$ and $\Delta_r G_x^{0'}$ values again show that the transfer of the first electron from fully reduced RBFH_2 ($x = 2$, blue lines) to α-FeOOH is thermodynamically less favorable than that of the second electron from the semiquinone species $\text{RBFH}^{\bullet}$ ($x = 1$, orange lines) to α-FeOOH. As for AQDS, we stipulate that the less exergonic, and above pH 6.6 even endergonic, first electron transfer from RBFH_2 and RBFH^- to α-FeOOH controls the overall rates of electron transfer from reduced riboflavin to α-FeOOH.

Relating Rates of Goethite Reduction by Reduced EES to Free Energies. We correlated the initial rates of goethite reduction that we determined experimentally for reactions with AQDSH_2^{2-} and RBFH_2 over the pH range 4.50 to 7.25 and 6.25 to 7.25, respectively, at 0.25-pH intervals with the corresponding $\Delta_r G_x^{0'}$ values calculated as described above. Surface area-normalized initial rates, r_{SA}, of goethite reduction were determined by spectrophotometrically following EES oxidation over time (examples for AQDSH_2^{2-} in Fig. 2 *A*–*C* and *SI Appendix*, Figs. S12*A* and S13, and examples for RBFH_2 in *SI Appendix*, Fig. S12*B*). We first relate r_{SA} values for AQDSH_2^{2-} and RBFH_2 to $\Delta_r G_{1,2}^{0'}$ values calculated by using the reduction potential averaged over both electrons transferred, $E_{\text{H},1,2}^{0'}$ (Fig. 2*D*). While r_{SA} values for AQDSH_2^{2-} and RBFH_2 decreased with increasing (i.e., less negative) $\Delta_r G_{1,2}^{0'}$ (Fig. 2*D*), we observed disparate trends between the two EES, consistent with the results of Shi et al. (25) According to our hypothesis, these disparate trends are artificial, as they result from relating rates to free energy measures of both electrons transferred. Indeed, when replotting r_{SA} versus $\Delta_r G_2^{0'}$ for the less exergonic of the two electron transfers from the reduced EES to Fe(III), all rate data for AQDSH_2^{2-} and RBFH_2 coalesce into one single relationship (Fig. 2*E*). Consequently, a disparity between the two EES datasets is again observed when plotting r_{SA} values against the free energy of the more exergonic, second electron transfer from the semiquinone species to Fe(III), $\Delta_r G_1^{0'}$ (Fig. 2*F*).

Reconciling Iron Oxide Reduction Rates by EES across Datasets. We demonstrate a broad applicability of the r_{SA}–$\Delta_r G_2^{0'}$ relationship by extending our evaluation to experimental systems with hematite and two additional EES, as well as by including literature-reported rates of goethite and hematite reduction by various EES (25, 38–40). Taken together, the resulting datasets include experiments with three two-electron EES (5-hydroxy-1,4-naphthalenedione [juglone], anthrahydroquinone-2,6-disulfonate, and riboflavin) and four viologen EES. We note that, contrary to the three two-electron EES, viologens exhibit an $E_{\text{H},1}^0$ above $E_{\text{H},2}^0$ (41), thus allowing formation of stable semiquinone species that act as one-electron transfer reductants of Fe(III). Rates of Fe(III) reduction by one-electron reduced viologens are therefore expected to follow the above free energy relationship for two-electron EES, but for viologens on the basis of relating rates to $\Delta_r G_1^{0'}$.

Fig. 3 *A* and *B* show initial rates of goethite and hematite reduction by the two-electron EES anthrahydroquinone-2,6-disulfonate, riboflavin, and juglone plotted versus $\Delta_r G_2^{0'}$. The figures also include rates of reduction by the four viologens (i.e., cyanomethylviologen, methylviologen, benzylviologen, and diquat) versus the free energy of the one-electron transfer from the viologen semiquinone to Fe(III), $\Delta_r G_1^{0'}$. Rates determined in this work are shown in colored symbols, whereas data from the literature (25, 38–40) are displayed in gray symbols. Values of r_{SA} for both goethite and hematite by the two-electron EES fell into well-constrained relationships with $\Delta_r G_2^{0'}$ with only few exceptions of some literature-reported data. The viologen-based r_{SA} data extended these relationships for the two-electron EES toward higher rates and more exergonic $\Delta_r G_1^{0'}$. The relationships not only hold for experiments which commonly are set up with fully reduced EES and in the absence of Fe(II) but

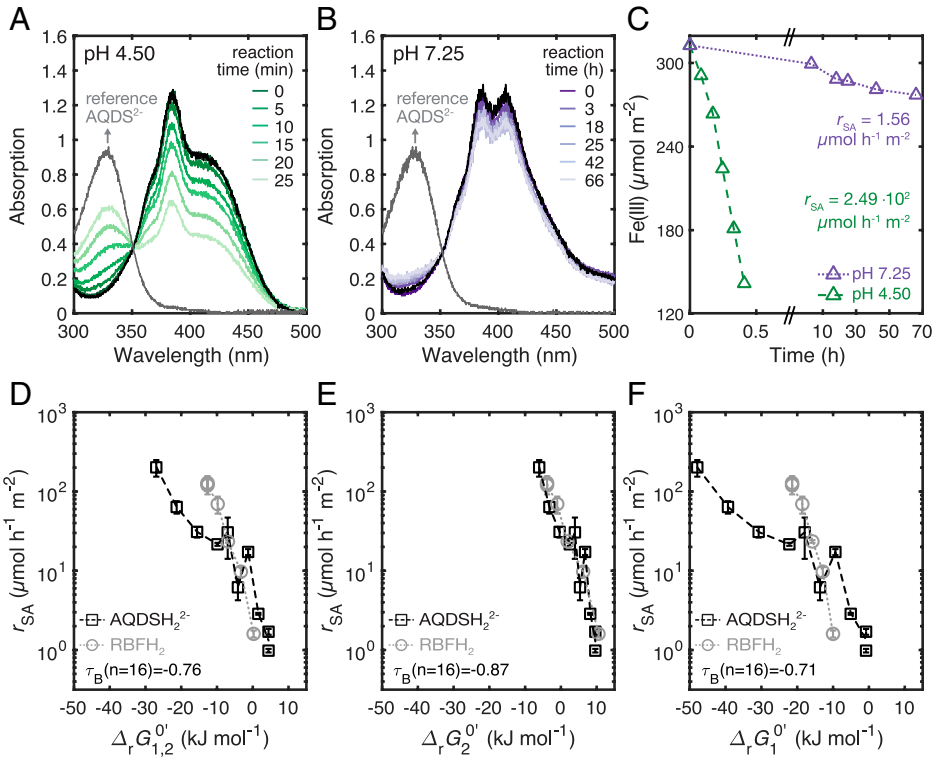

Fig. 2. Selected data from goethite reduction experiments with reduced AQDS and riboflavin ($RBFH_2$). (*A* and *B*) Absorbance spectra of mixtures of oxidized ($AQDS^{2-}$) and reduced AQDS ($AQDSH_2^{2-}$) collected during experiments at pH 4.50 and 7.25. (*C*) Changes in Fe(III) concentrations normalized to initial goethite surface area over time in the two experiments. Experiments were designed such that equal electron equivalents of Fe(III) and $AQDSH_2^{2-}$ were present at all times. Fe(III) concentrations were therefore determined directly from the changes in the absorption spectra shown in *A* and *B* by deconvolution as described in *Materials and Methods*. Surface area-normalized initial rates of Fe(III) reduction, r_{SA}, for goethite were derived from changes of Fe(III) concentrations according to Eq. **12** (*SI Appendix*, Fig. S13). (*D–F*) r_{SA} values measured at pH 4.50 to 7.25 for $AQDSH_2^{2-}$ and pH 6.25 to 7.25 for $RBFH_2$ versus $\Delta_r G_x^{0'}$, where x refers to the free energy of (*D*) the two-electron transfer from the reduced EES to Fe(III) (x = 1,2), (*E*) the first one-electron transfer from the hydroquinone species of the EES to Fe(III) (x = 2), and (*F*) the second one-electron transfer from the semiquinone species of the EES to Fe(III) (x = 1). Error bars represent deviations from the mean of duplicate measurements. Kendall's τ_B values from rank correlation analysis are reported for the number of data points (n) used in the statistical analysis (–1 = perfect negative correlation, 0 = no correlation). *SI Appendix*, Fig. S6 *A* and *B* shows the same r_{SA} values versus pH.

also for systems in which the iron oxides are partially reduced, as typically found in the natural environment: Reduction rates that we measured at varying initial Fe(II) concentrations and thereby modulated thermodynamic driving force also fell into these relationships (*SI Appendix*, Figs. S8 and S9). By comparison, plotting the reduction rates by the two-electron EES versus $\Delta_r G_{1,2}^{0'}$ resulted in scattered data without a consistent trend for the different EES (Fig. 3 *C* and *D*). We also observed a pronounced offset of the r_{SA} values toward more negative $\Delta_r G_{1,2}^{0'}$ relative to r_{SA} values obtained for the viologen single-electron transfer reductants. Our finding that r_{SA} values collected over a wide range of experimental conditions and mineral morphologies (i.e., different EES, varying ratios of Fe(III) to EES concentration, iron oxide crystal sizes and shapes, and solution pH) exhibited the same dependence on $\Delta_r G_2^{0'}$ confirms that rates of Fe(III) reduction by EES correlate with thermodynamic descriptors of the first, one-electron transfer from the fully reduced EES to Fe(III).

While we present these principles with data for pH 4 to 8, we expect that the established free energy relationship also applies outside this pH range and for other potentially relevant two-electron transfer EES such as pyocyanines (17). Note that, at $pH > 8$ for quinones and flavins and at $pH < 5$ for pyocyanines, semiquinone species are stable because these EES have higher $E_{H,1}^0$ than $E_{H,2}^0$ (34). It follows from the above reasoning that, under such conditions, rates of iron oxide reduction are expected to correlate with $\Delta_r G_1^0$ instead of $\Delta_r G_2^0$, a behavior that we observed in experiments with viologens.

Free Energy Relationships for Fe(III) Oxide Reduction in a Biogeochemical Context. Comparing the kinetics of Fe(III) reduction by EES on a thermodynamic basis allows one to systematically assess the relative importance of this process to anaerobic respiration pathways across systems with different biogeochemical conditions. In fact, the free energy relationships in Fig. 3 *A* and *B* integrate over a range of elementary processes and iron oxide thermodynamic properties that all contribute to the observable reduction rates. The potential processes and properties that cause higher reduction rates of hematite than goethite at $\Delta_r G_2^{0'} > -20\ kJ \cdot mol^{-1}$ include the following: 1) higher density of reactive surface hydroxyl sites (42, 43) on hematite (44) than goethite (42) crystal faces at which interfacial electron transfer to Fe(III) occurs, 2) larger reactive surface area of hematite than goethite resulting from differences in particle aggregation (45), 3) larger number of surface defects and hence more efficient electron transfer to structural Fe(III) in hematite than goethite (46), 4) smaller band gap and hence more efficient electron transfer inside hematite than goethite crystals (47, 48), and 5) variations in the distribution and reactivity toward reduction of different crystal faces in hematite and goethite (49, 50).

Despite differences in the free energy relationships between hematite and goethite, reduction rates of both iron oxides asymptotically approach a maximum value of $r_{SA} \approx 5 \cdot 10^3 \mu\ mol \cdot h^{-1} \cdot m^{-2}$ at $\Delta_r G_2^{0'} < -20\ kJ \cdot mol^{-1}$. This rate is approximately three orders of magnitude lower than estimated rates of EES diffusion to the oxide surface (estimated at $10^6 \mu\ mol \cdot h^{-1} \cdot m^{-2}$

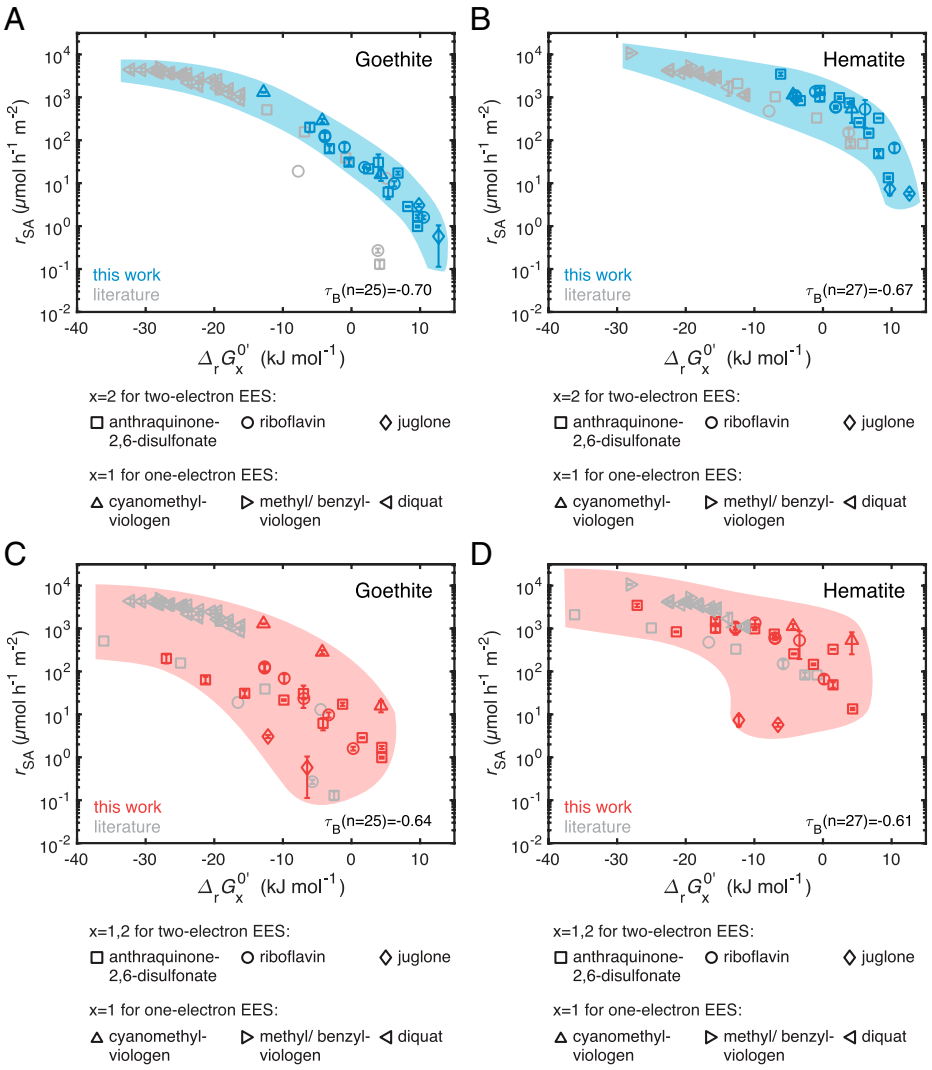

Fig. 3. Free energy relationships for the rates of goethite and hematite reduction by EES. (*A* and *B*) Surface area-normalized initial reduction rates, r_{SA}, for goethite and hematite with reduced one- and two-electron EES versus the free energy of the one-electron transfer from the semiquinone species of one-electron EES ($\Delta_r G_1^{0'}$) and first one-electron transfer from reduced two-electron EES ($\Delta_r G_2^{0'}$) to the iron oxide. The r_{SA} values from the literature are shown in gray (see *SI Appendix*, sections S1 and S5 for thermodynamic calculations) (25, 38–40). The three literature r_{SA} values in *A* which are smaller than expected based on the free energy relationship were determined from measurements of dissolved Fe(II) at near-neutral pH and therefore may have underestimated the rates of electron transfer (*SI Appendix*, section S1). (*C* and *D*) The identical r_{SA} values vs. the free energy of the two-electron transfer from the EES to the iron oxide ($\Delta_r G_{1,2}^{0'}$). Data for one-electron EES are replotted from *A* and *B*. *SI Appendix*, Figs. S6 and S7 shows r_{SA} values versus pH. Blue and red areas serve as visual guides for the quality of the correlation of kinetic and thermodynamic data. Error bars represent deviations from the mean of duplicate measurements. Kendall's τ_B values from rank correlation analysis for the two-electron EES data are reported for the number of data points (n) used in the statistical analysis (–1 = perfect negative correlation, 0 = no correlation).

for our reactors; *SI Appendix*, Fig. S10) but falls into the range of reported rates of electron transfer from Fe(II) complexes on oxide surfaces to Fe(III) in the crystal lattice (51, 52). This comparison suggests that the electron transfer into the crystal lattice rather than rates of EES diffusion toward the oxide surface governed the maximum reduction rates measured herein. The detachment of Fe(II) from the iron oxide surface, which has previously been considered the rate-limiting step for iron oxide reductive dissolution (53–55), proceeds at rates of $\sim 10^{-1}\,\mu\,\mathrm{mol}\cdot\mathrm{h}^{-1}\cdot\mathrm{m}^{-2}$ (51). We measured similarly small r_{SA} values under the least favorable thermodynamic conditions (i.e., $\Delta_r G_2^{0'} > 10\,\mathrm{kJ}\cdot\mathrm{mol}^{-1}$).

Implications. Our work presents a conceptual framework that allows to relate measured rates of EES-mediated microbial respiration using crystalline iron oxides to the underlying thermodynamics of the electron transfer from the EES to Fe(III)-bearing solids. The framework advances our capabilities to assess the efficacy of this microbial respiration pathway, particularly when applied to (laboratory) model systems that are well characterized with regards to iron-reducing microorganisms, EES, iron oxide mineralogy, and pH. In such systems, measured reduction rates may provide estimates for the reaction free energy and thus the reduction potential to which microbes reduced the EES. If the oxidized and reduced EES species are analytically accessible, the reduction potential of the EES can be computed and compared to the E_H of the EES inferred from the experimental reduction rates. Agreement between measured and predicted rates would help to elucidate which fundamental step in Fe(III) reduction controls the overall rate (see above), whereas disagreement would point at either kinetic limitations (e.g., rates of microbial EES reduction or EES diffusion) or

enhanced reactivities (e.g., by favorable pH in the microbial biofilm on iron oxide surfaces that deviate from bulk solution pH). Such deviations would therefore be highly informative to aid in the identification and interpretation of potentially limiting and enhancing factors to EES-mediated iron oxide respiration. When extending free energy relationships from goethite and hematite to other iron-bearing minerals (e.g., lepidocrocite, magnetite, six-line ferrihydrite, and clay minerals), relative microbial reduction rates of these minerals in the presence of EES in mixed mineral systems can be interpreted by considering the underlying reaction thermodynamics. Similarly, in systems that contain iron-reducing microorganisms which utilize electron transfer pathways other than EES (e.g., nanowires or direct electron transfer), reaction thermodynamics allow assessing rates of EES-mediated iron oxide reduction and thus the relative competitiveness of this respiration pathway. Finally, in engineered applications, such as microbial fuel cells, the framework developed herein lays the foundation to identify EES that are highly effective to catalyze electron transfer from the microbial cells to the electrode.

We anticipate that the identical driving-force dependence also applies for the kinetics of EES reduction at microbial cell surfaces, for example, by membrane-bound multiheme cytrochrome proteins (15, 22, 23, 56, 57). In analogy to the above consideration for electron transfers from the EES to Fe(III) oxides, electron transfer rates from such proteins to the EES would be thermodynamically controlled by the one-electron reduction potential of the oxidized quinone species, $E_{H,1}$. In fact, metal-reducing bacteria such as *Shewanella* sp. sustain different combinations of outer-membrane c-type cytochromes with bound cell-secreted flavins poised to increase the E_H of flavin quinone/semiquinone redox couples for one-electron transfer reactions with solid and dissolved electron donors and acceptors (15, 22, 23). From a thermodynamic perspective, the ability of microorganisms to elevate the $E_{H,1}$ of the quinone/semiquinone redox couple either by binding the EES or by modulation of the pH in their near cell-surface microenvironments might constitute a competitive advantage for effective respiration onto two-electron transfer EES and thus Fe(III) oxides.

Materials and Methods

Solutions and Iron Oxide Suspensions. All solutions and iron oxide suspensions were prepared with doubly deionized water (DDW, resistivity $>$ 18.2 MΩ· cm, Barnstead Nanopure Diamond Water Purification System) and were purged with ultrahigh purity N_2 (99.999%) for at least 3 h prior to transfer into an anoxic glovebox (Unilab 2000, MBraun, N_2 atmosphere with $<$ 2 ppm O_2). A list of all chemicals used is provided in *SI Appendix*, section S2. Iron oxide reduction experiments were performed in pH-buffered solutions containing 0.1 M buffering agent (i.e., acetic acid [$pK_a = 4.75$] for experiments at pH 4.50 to 5.00, 2-(*N*-morpholino)ethanesulfonic acid [MES; $pK_a = 6.15$] at pH 5.50 to 6.25, and 3-morpholinopropane-1-sulfonic acid [$pK_a = 7.2$] at pH 6.50 to 7.25).

Synthesis and Characterization of Iron Oxides. We synthesized goethite and hematite using established protocols (58). In brief, goethite was synthesized by dissolving 80.8 g $Fe(NO_3)_3 \cdot 9H_2O$ in 200 mL of DDW, adding 180 mL of 5 M KOH under stirring and diluting with DDW to 2 L. The resulting suspension was held at 70 °C for 60 h and was subsequently washed with DDW by repeated centrifugation to remove electrolytes. Hematite was synthesized by adding 8.08 g $Fe(NO_3)_3 \cdot 9H_2O$ to 2 L of a 2-mM HNO_3 solution heated to 98 °C. The resulting precipitate was aged at 98 °C for 7 d and subsequently washed with DDW by repeated centrifugation. We confirmed the identity and purity of the iron oxides by X-ray diffraction, X-ray absorption spectroscopy, and Mössbauer spectroscopy (40). The specific surface areas of goethite and hematite were 36 and 46 $m^2 \cdot g^{-1}$, respectively, as determined by N_2-BET analysis (Nova 3200e, Quantachrome). Exemplary electron microscopy images of the goethite and hematite particles are provided in *SI Appendix*, Fig. S11. Goethite and hematite were stored as suspensions in DDW at 4 °C until being used in the iron oxide reduction experiments.

Reduction of EES. We obtained the hydroquinone (fully reduced) species of AQDS, riboflavin (7,8-dimethyl-10-[(2S,3S,4R)-2,3,4,5-tetrahydroxypentyl] benzo[g]pteridine-2,4-dione), and juglone (5-hydroxy-1,4-naphthalenedione) and the stable semiquinone species of cyanomethylviologen (1,1′-Bis(cyanomethyl)-4,4′-bibyridinium dibromide) by controlled potential bulk electrolysis (potentiostat 1000C, CH Instruments) of the corresponding oxidized species (see *SI Appendix*, Figs. S1–S4 for the molecular structures of the EES). Bulk electrolysis was performed inside an anoxic glove box in a set of independent electrochemical cells each consisting of a 25-mL glassy carbon working electrode cylinder (Sigradur G, HTW), a platinum wire counterelectrode that was separated from the working electrode compartment by a porous glass frit (PORE E tubes; ACE glass), and an Ag/AgCl reference electrode (Re1B, ALS). EES solutions were prepared (4 mM electron equivalents in a solution buffered to pH 6.00 containing 0.02 M MES and 0.01 M KCl) and reduced in the electrochemical cells under stirring at applied reduction potentials 0.12 V lower than the reduction potential of the first electron transferred during EES reduction at pH 6.00. At these applied reduction potentials, EES were fully reduced ($\geq$97%), as confirmed spectrophotometrically.

Iron Oxide Reduction Experiments. Duplicate iron oxide reduction experiments were performed at each tested solution condition under an anoxic atmosphere in a glove box at 25 ± 3 °C. Experiments were performed in 15-mL glass vials that were shielded from light to rule out photochemical side reactions. Iron oxide suspensions were prepared by diluting the goethite and hematite stock suspensions (4 mM Fe(III)) into the experimental buffers to final concentrations of 0.32 mM Fe(III) (experiments with AQDS) or 0.16 mM Fe(III) (experiments with all other EES). These suspensions were equilibrated for 1 h under stirring before being split into duplicate reactors. Fe(III) reduction was initiated by addition of the EES to the reactors to final concentrations of 0.32 mM electron equivalents (experiments with AQDS) or 0.16 mM electron equivalents (experiments with all other EES). The suspension volume in the reactors at the onset of the experiments was 10 mL. We chose EES and Fe(III) concentrations for experiments with AQDS to be twice as high than for the other EES because of the comparatively lower molar absorption coefficients of reduced and oxidized AQDS. The suspensions in the reactors were continuously stirred (350 rpm) using Teflon-coated stir bars. At multiple time points during the experiments, 0.9-mL suspension aliquots were collected from the reactors using plastic syringes, and the reaction in these aliquots was immediately quenched by removing iron oxide particles by syringe filtration (0.22 μm, cellulose acetate, BGB Analytics). For experiments with juglone, polyvinylidene filters were used (0.22 μm, BGB Analytics) because juglone sorbed to cellulose acetate filters that we used for all other EES. We spectrophotometrically followed the oxidation of the reduced EES species over the course of the experiments. Absorption spectra of the filtered suspension aliquots were recorded in ultraviolet (UV) cuvettes (Semadeni) from 250 to 800 nm using a spectrophotometer (detector USB4000-UV-VIS light source DH-2000-BAL, software Ocean View; all Ocean Optics) inside the anoxic glove box in which reaction kinetics were followed. Reference absorption spectra of the reduced and oxidized EES species were also recorded at each experimental pH. Absorption spectra collected over the course of all experiments showed isosbestic points. Total dissolved EES concentrations remained constant over the course of the experiments, implying that there was, at most, minor sorption of EES to iron oxide surfaces. We note that the ratio of reduced EES to Fe(III) of 1:1 in our experiments presumably resulted in saturation of iron oxide surfaces with EES. We also note that ferrous hydroxide likely did not form in our experiments, given that its solubility product was not reached even at the highest Fe(II) concentration of 0.32 mM and the highest pH 7.25. Lastly, we note that we did not follow the reduction of Fe(III) by quantifying the production of dissolved Fe(II) for the following reasons: 1) The reductive dissolution of iron oxides consists of several elementary reactions which include (i) precursor complex formation of EES with Fe(III) on the oxide surface; (ii) electron transfer from the EES to Fe(III); (iii) release of the oxidized EES; and (iv) oxide surface protonation, release of Fe(II), and reexposure of Fe(III) on the oxide surface (59). This implies that the rate of electron transfer can be much higher than the rate of dissolved Fe(II) formation. Hence, quantifying the formation rate of the oxidized EES instead of the formation of dissolved Fe(II) is the most direct measure of electron transfer from the EES to the Fe(III). 2) Fe(II) formed during Fe(III) reduction may not desorb from the mineral surface or readsorb from solution to the mineral surface. In this case, analyzing only dissolved Fe(II) underestimates the rates of Fe(III) reduction. 3) The electron transfer step can be so fast that it is not accessible through withdrawing aliquots for determining total Fe(II). The addition of Fe(II) complexing agents to the iron oxide–containing suspension is not a viable option because such procedures would alter the iron redox equilibrium toward Fe(II) formation and thus lead to an overestimation of the amount of Fe(II) present.

Data Analysis. We determined the fractions of oxidized and reduced EES species at each sampling point by deconvoluting the collected absorption spectrum into the relative contributions of the fully oxidized and fully reduced EES species for two-electron EES and the reduced and semiquinone species for one-electron EES using the Spectr-O-Matic toolbox in Matlab (60) (MathWorks, code in *SI Appendix*, section S3). We did not consider the semiquinone EES species of the two-electron EES in the deconvolution because the semiquinone species is transient and hence not visible in the absorption spectra. Exemplary absorbance spectra of the different EES collected over the course of the iron oxide reduction experiments are presented in Fig. 2 *A* and *B* and *SI Appendix*, Fig. S12.

We determined initial rates of iron oxide reduction (moles per liter per hour) using a pseudo-first-order rate law, as described in *SI Appendix*, section S4. We designed the experiments such that equal electron equivalents of Fe(III) and EES were present at all reaction times. This experimental design allowed us to quantify observed iron oxide reduction rate constants, k_{obs} (per hour), from a linear fit of ($1/f_{red}$) versus time (Eq. **11**).

$$\frac{1}{f_{red}} = 1 + k_{obs} \cdot t \qquad [11]$$

where f_{red} is the fraction of reduced EES at time t. Fitting was performed from the onset of iron oxide reduction until 10% of the added EES had become oxidized. Because the transfer of electrons from the EES to the iron oxide occurs at the oxide surface, we normalized iron oxide reduction rates to specific iron oxide surface area (SA), r_{SA} (moles per square meter per hour), according to Eq. **12**.

$$r_{SA} = \frac{k_{obs}}{SA \cdot M_w} \qquad [12]$$

where SA = 36 $m^2 \cdot g^{-1}$ for goethite and 46 $m^2 \cdot g^{-1}$ for hematite, and M_w is the molar mass of goethite and hematite per Fe(III) (i.e., M_w = 88.85 $g \cdot mol^{-1}_{Fe(III)}$ for goethite [α-FeOOH] and M_w = 79.85 $g \cdot mol^{-1}_{Fe(III)}$ for hematite [α-Fe_2O_3]).

Thermodynamic Calculations. We calculated the free energies of the first and second electron transfer from the reduced EES to goethite and hematite as well as the free energies averaged over both electron transfers. For these calculations, we used the half reactions for the reductive dissolution of goethite (α- FeOOH) and hematite (α- Fe_2O_3) (Eqs. **13** and **14**),

$$\alpha\text{-FeOOH} + e^- + 3H^+ \rightleftharpoons Fe^{2+} + 2H_2O \qquad E_H(\text{goethite}) \qquad [13]$$

$$\alpha\text{-}Fe_2O_3 + 2e^- + 6H^+ \rightleftharpoons 2Fe^{2+} + 3H_2O \qquad E_H(\text{hematite}) \qquad [14]$$

and the half-reaction for EES oxidation averaged over the two electron transfers (Eq. **15**) as well as the two individual one-electron transfer half-reactions (Eqs. **16** and **17**),

$$A + 2e^- + (y+z)H^+ \rightleftharpoons AH_{y+z}^{y+z-2} \qquad E_{H,1,2}(\text{shuttle}) \qquad [15]$$

$$A + e^- + yH^+ \rightleftharpoons AH_y^{\bullet(y-1)} \qquad E_{H,1}(\text{shuttle}) \qquad [16]$$

$$AH_y^{\bullet(y-1)} + e^- + zH^+ \rightleftharpoons AH_{y+z}^{y+z-2} \qquad E_{H,2}(\text{shuttle}) \qquad [17]$$

where A is the quinone, AH_{y+z}^{y+z-2} is the hydroquinone, and $AH_y^{\bullet(y-1)}$ is the semiquinone species of the EES, y is the number of protons transferred during the reduction of A to $AH_y^{\bullet(y-1)}$ (which depends on the pK_a of the semiquinone species and the experimental pH), and z is the number of protons transferred during the reduction of $AH_y^{\bullet(y-1)}$ to AH_{y+z}^{y+z-2} (which depends on the pK_a of the hydroquinone species and the experimental pH). In the calculations of free energies averaged over both electron transfers, we used the same reduction potentials of Fe(III) in goethite and hematite for both of the two sequential one-electron transfers. However, we accounted for the fact that the reduction potential of the iron oxides decreases over the course of the iron oxide reduction experiments due to the formation of dissolved ferrous iron, as shown below. The reduction potentials of the EES, $E_{H,x}$ (EES), associated with the first ($x = 1$) and second ($x = 2$) electron transferred during EES reduction and the reduction potential averaged over both electrons transferred (x = 1,2) are marked in Eqs. **15**–**17**. By convention, $x = 1$ and $x = 2$ refer to the order of electron transfer in the reductive direction. This implies that $x = 2$ and $x = 1$ are the first and second electron transferred during oxidation of the reduced EES (i.e., the order is reversed in the oxidative direction).

We used the Nernst equation to calculate the reduction potentials associated with reaction Eqs. **13**–**17** under experimental conditions and calculated the Gibbs free energy, $\Delta_r G_x^{0'}$ (kilojoules per mole electrons transferred), for iron oxide reductive dissolution from the difference in reduction potentials between the oxide and the EES according to Eq. **18**.

$$\Delta_r G_x^{0'} = -nF\left(E_H^{0'}(\text{oxide}) - E_{H,x}^{0'}\right) \qquad [18]$$

where n is the number of electrons transferred ($n = 1$ for the reduction of ferric to ferrous iron), F is the Faraday constant, and E_H (oxide) and $E_{H,x}$ are the reduction potentials of the iron oxide and the EES, respectively, at experimental pH and ferrous iron concentration. The subscript $_x$ refers to the first ($x = 1$) and second ($x = 2$) electron transferred during EES reduction and the average over both electrons transferred (x = 1,2). Inserting the Nernst equation for E_H (oxide) into Eq. **18** yields Eq. **19**.

$$\Delta_r G_x^{0'} = -nF\left(E_H^0(\text{oxide}) - 2.303\frac{RT}{F}\left(\log\{Fe_{aq}^{2+}\} + 3\ pH\right) - E_{H,x}^{0'}\right) \qquad [19]$$

where E_H^0(oxide) is the standard reduction potential of the iron oxide [E_H^0(oxide) = 0.768 V (37) and 0.769 V (37) for goethite and hematite, respectively], R is the gas constant, T is the absolute temperature, $\{Fe_{aq}^{2+}\}$ is the activity of dissolved Fe^{2+} (calculated for the time point at which 10% of the added Fe(III) had become reduced and assuming that all Fe(II) was dissolved), and $E_{H,x}^{0'}$ is the reduction potential of the EES at experimental pH (*SI Appendix*, Fig. S5). The calculation of $E_{H,x}^{0'}$ values is described in detail in *SI Appendix*, section S5. In brief, we calculated reduction potentials of the quinone/hydroquinone ($E_{H,1,2}^{0'}$) and quinone/semiquinone ($E_{H,1}^{0'}$) redox couples from published reduction potentials for AQDS (31, 34), riboflavin (33, 36), juglone (32, 61), and cyanomethylviologen (62) (*SI Appendix*, Table S1). Reduction potentials of the semiquinone/hydroquinone redox couples ($E_{H,2}^{0'}$) were not available for all EES, and we thus calculated them from $E_{H,1,2}^{0'}$ and $E_{H,1}^{0'}$ (given that $E_{H,1,2}^{0'}$ is the average of $E_{H,1}^{0'}$ and $E_{H,2}^{0'}$). In all of these calculations, we assumed equal activities of the hydroquinone, quinone, and semiquinone species of the EES because we could not experimentally quantify semiquinone concentrations.

Rank Correlation Analysis. We performed Kendall rank correlation analysis on the r_{SA} and $\Delta_r G_x^{0'}$ datasets to confirm the tighter relationship between goethite and hematite reduction rates and free energy of the first electron transferred ($\Delta_r G_2^{0'}$) as compared to the free energies averaged over both electron transferred ($\Delta_r G_{1,2}^{0'}$) and the second electron transferred ($\Delta_r G_1^{0'}$). In the analysis, we included data for two-electron EES only. Correlation analysis was performed using the corr function in Matlab (MathWorks). Kendall's τ_B values and number of data points included in the analysis are reported in Figs. 2 and 3. A value of $\tau_B = -1$ signifies a perfect negative relationship, and $\tau_B = 0$ signifies no relationship.

Data Availability. Raw data for UV-Vis measurements, figures illustrating the deconvolution and rate fits performed on raw data, the file with all rate and free energy values, and codes for data analysis have been deposited in Eawag Research Data Institutional Repository (https://doi.org/10.25678/0002C2).

ACKNOWLEDGMENTS. We thank Ralf Kaegi for his help with electron microscopy analysis, Numa Pfenninger for technical and analytical support, and the Swiss National Science Foundation for financial support (Grant 200021_149283).

1. A. Kappler *et al.*, An evolving view on biogeochemical cycling of iron. *Nat. Rev. Microbiol.* **19**, 360–374 (2021).
2. T. Borch *et al.*, Biogeochemical redox processes and their impact on contaminant dynamics. *Environ. Sci. Technol.* **44**, 15–23 (2010).
3. J. Majzlan, "Minerals and aqueous species of iron and manganese as reactants and products of microbial metal respiration" in *Microbial Metal Respiration*, J. Gescher, A. Kappler, Eds. (Springer, Berlin, Germany, 2013), pp. 1–28.
4. D. R. Lovley, D. E. Holmes, K. P. Nevin, Dissimilatory Fe(III) and Mn(IV) reduction. *Adv. Microb. Physiol.* **49**, 219–286 (2004).
5. R. M. Cornell, U. Schwertmann, *The Iron Oxides: Structure, Properties, Reactions, Occurrences and Uses*, R. M. Cornell, U. Schwertmann, Eds. (Wiley-VCH Verlag, Weinheim, Germany, ed. 2, rev. and extended, 2003).
6. B. Thamdrup, "Bacterial manganese and iron reduction in aquatic sediments" in *Advances in Microbial Ecology*, B. Schink, Ed. (Springer, Boston, MA, 2000), pp. 41–84.
7. S. Freguia, M. Masuda, S. Tsujimura, K. Kano, *Lactococcus lactis* catalyses electricity generation at microbial fuel cell anodes via excretion of a soluble quinone. *Bioelectrochemistry* **76**, 14–18 (2009).
8. K. P. Nevin, D. R. Lovley, Potential for nonenzymatic reduction of Fe(III) via electron shuttling in subsurface sediments. *Environ. Sci. Technol.* **34**, 2472–2478 (2000).

9. D. K. Newman, R. Kolter, A role for excreted quinones in extracellular electron transfer. *Nature* **405**, 94–97 (2000).
10. D. R. Monteverde *et al.*, Distribution of extracellular flavins in a coastal marine basin and their relationship to redox gradients and microbial community members. *Environ. Sci. Technol.* **52**, 12265–12274 (2018).
11. S. H. Light *et al.*, A flavin-based extracellular electron transfer mechanism in diverse Gram-positive bacteria. *Nature* **562**, 140–144 (2018).
12. E. D. Brutinel, J. A. Gralnick, Shuttling happens: Soluble flavin mediators of extracellular electron transfer in *Shewanella*. *Appl. Microbiol. Biotechnol.* **93**, 41–48 (2012).
13. E. Marsili *et al.*, *Shewanella* secretes flavins that mediate extracellular electron transfer. *Proc. Natl. Acad. Sci. U.S.A.* **105**, 3968–3973 (2008).
14. H. von Canstein, J. Ogawa, S. Shimizu, J. R. Lloyd, Secretion of flavins by *Shewanella* species and their role in extracellular electron transfer. *Appl. Environ. Microbiol.* **74**, 615–623 (2008).
15. A. Okamoto, K. Hashimoto, K. H. Nealson, R. Nakamura, Rate enhancement of bacterial extracellular electron transport involves bound flavin semiquinones. *Proc. Natl. Acad. Sci. U.S.A.* **110**, 7856–7861 (2013).
16. K. Michelson, R. E. Alcalde, R. A. Sanford, A. J. Valocchi, C. J. Werth, Diffusion-based recycling of flavins allows *Shewanella oneidensis* MR-1 to yield energy from metal reduction across physical separations. *Environ. Sci. Technol.* **53**, 3480–3487 (2019).
17. N. R. Glasser, S. H. Saunders, D. K. Newman, The colorful world of extracellular electron shuttles. *Annu. Rev. Microbiol.* **71**, 731–751 (2017).
18. Y. Wang, S. E. Kern, D. K. Newman, Endogenous phenazine antibiotics promote anaerobic survival of *Pseudomonas aeruginosa* via extracellular electron transfer. *J. Bacteriol.* **192**, 365–369 (2010).
19. A. Price-Whelan, L. E. P. Dietrich, D. K. Newman, Rethinking 'secondary' metabolism: Physiological roles for phenazine antibiotics. *Nat. Chem. Biol.* **2**, 71–78 (2006).
20. L. Shi *et al.*, Extracellular electron transfer mechanisms between microorganisms and minerals. *Nat. Rev. Microbiol.* **14**, 651–662 (2016).
21. E. D. Brutinel, J. A. Gralnick, "On the role of endogenous electron shuttles in extracellular electron transfer" in *Microbial Metal Respiration*, J. Gescher, A. Kappler, Eds. (Springer, Berlin, Germany, 2013), pp. 83–105.
22. A. Okamoto, K. Hashimoto, K. H. Nealson, Flavin redox bifurcation as a mechanism for controlling the direction of electron flow during extracellular electron transfer. *Angew. Chem. Int. Ed. Engl.* **53**, 10988–10991 (2014).
23. A. Okamoto *et al.*, Cell-secreted flavins bound to membrane cytochromes dictate electron transfer reactions to surfaces with diverse charge and pH. *Sci. Rep.* **4**, 5628 (2014).
24. M. Wolf, A. Kappler, J. Jiang, R. U. Meckenstock, Effects of humic substances and quinones at low concentrations on ferrihydrite reduction by *Geobacter metallireducens*. *Environ. Sci. Technol.* **43**, 5679–5685 (2009).
25. Z. Shi, J. M. Zachara, Z. Wang, L. Shi, J. K. Fredrickson, Reductive dissolution of goethite and hematite by reduced flavins. *Geochim. Cosmochim. Acta* **121**, 139–154 (2013).
26. Y. Wang, D. K. Newman, Redox reactions of phenazine antibiotics with ferric (hydr)oxides and molecular oxygen. *Environ. Sci. Technol.* **42**, 2380–2386 (2008).
27. C. Liu, J. M. Zachara, N. S. Foster, J. Strickland, Kinetics of reductive dissolution of hematite by bioreduced anthraquinone-2,6-disulfonate. *Environ. Sci. Technol.* **41**, 7730–7735 (2007).
28. Z. Shi *et al.*, Redox reactions of reduced flavin mononucleotide (FMN), riboflavin (RBF), and anthraquinone-2,6-disulfonate (AQDS) with ferrihydrite and lepidocrocite. *Environ. Sci. Technol.* **46**, 11644–11652 (2012).
29. R. Marcus, N. Sutin, Electron transfers in chemistry and biology. *Biochim Biophys. Acta Rev. Bioenerg.* **811**, 265–322 (1985).
30. M. Uchimiya, A. T. Stone, Redox reactions between iron and quinones: Thermodynamic constraints. *Geochim. Cosmochim. Acta* **70**, 1388–1401 (2006).
31. H. Pal, D. K. Palit, T. Mukherjee, J. P. Mittal, One-electron reduction of anthraquinone sulphonates: A pulse radiolysis study. *Int. J. Radiat. Appl. Instrum. C. Radiat. Phys. Chem.* **37**, 227–235 (1991).
32. T. Mukherjee, One-electron reduction of juglone (5-hydroxy-1,4-naphthoquinone): A pulse radiolysis study. *Int. J. Radiat. Appl. Instrum. C. Radiat. Phys. Chem.* **29**, 455–462 (1987).
33. R. F. Anderson, Energetics of the one-electron reduction steps of riboflavin, FMN and FAD to their fully reduced forms. *Biochim. Biophys. Acta* **722**, 158–162 (1983).
34. W. M. Clark, *Oxidation Reduction Potentials of Organic Systems* (Williams and Wilkins, Baltimore, MD, 1960).
35. S. G. Mayhew, The effects of pH and semiquinone formation on the oxidation-reduction potentials of flavin mononucleotide. A reappraisal. *Eur. J. Biochem.* **265**, 698–702 (1999).
36. R. M. C. Dawson, W. H. Elliott, D. C. Elliott, *Data for Biochemical Research* (Oxford University Press, New York, NY, 1960).
37. C. A. Gorski, R. Edwards, M. Sander, T. B. Hofstetter, S. M. Stewart, Thermodynamic characterization of iron oxide-aqueous Fe^{2+}redox couples. *Environ. Sci. Technol.* **50**, 8538–8547 (2016).
38. W. D. Burgos *et al.*, Reaction-based modeling of quinone-mediated bacterial iron(III) reduction. *Geochim. Cosmochim. Acta* **67**, 2735–2748 (2003).
39. D. E. Ross, S. L. Brantley, M. Tien, Kinetic characterization of OmcA and MtrC, terminal reductases involved in respiratory electron transfer for dissimilatory iron reduction in *Shewanella oneidensis* MR-1. *Appl. Environ. Microbiol.* **75**, 5218–5226 (2009).
40. M. Aeppli, A. Voegelin, C. A. Gorski, T. B. Hofstetter, M. Sander, Mediated electrochemical reduction of iron (oxyhydr-)oxides under defined thermodynamic boundary conditions. *Environ. Sci. Technol.* **52**, 560–570 (2018).
41. C. L. Bird, A. T. Kuhn, Electrochemistry of the viologens. *Chem. Soc. Rev.* **10**, 49–82 (1981).
42. M. Villalobos, M. A. Cheney, J. Alcaraz-Cienfuegos, Goethite surface reactivity: II. A microscopic site-density model that describes its surface area-normalized variability. *J. Colloid Interface Sci.* **336**, 412–422 (2009).
43. V. Barrón, J. Torrent, Surface hydroxyl configuration of various crystal faces of hematite and goethite. *J. Colloid Interface Sci.* **177**, 407–410 (1996).
44. S. V. Yanina, K. M. Rosso, Linked reactivity at mineral-water interfaces through bulk crystal conduction. *Science* **320**, 218–222 (2008).
45. D. M. Cwiertny, R. M. Handler, M. V. Schaefer, V. H. Grassian, M. M. Scherer, Interpreting nanoscale size-effects in aggregated Fe-oxide suspensions: Reaction of Fe(II) with Goethite. *Geochim. Cosmochim. Acta* **72**, 1365–1380 (2009).
46. V. Alexandrov, K. M. Rosso, Ab initio modeling of Fe(II) adsorption and interfacial electron transfer at goethite (α-FeOOH) surfaces. *Phys. Chem. Chem. Phys.* **17**, 14518–14531 (2015).
47. M. Sharma, S. Murugavel, D. K. Shukla, F. M. F. D. Groot, Reversal in the lattice contraction of α-Fe_2O_3 nanoparticles. *J. Phys. Chem. C* **122**, 9292–9301 (2018).
48. H. Zhang *et al.*, Size-dependent bandgap of nanogoethite. *J. Phys. Chem. C* **115**, 17704–17710 (2011).
49. S. Hu, Y. Wu, Z. Shi, F. Li, T. Liu, Quinone-mediated dissimilatory iron reduction of hematite: Interfacial reactions on exposed 001 and 100 facets. *J. Colloid Interface Sci.* **583**, 544–552 (2021).
50. S. Chatman, P. Zarzycki, K. M. Rosso, Surface potentials of (001), (012), (113) hematite (α-Fe_2O_3) crystal faces in aqueous solution. *Phys. Chem. Chem. Phys.* **15**, 13911–13921 (2013).
51. P. Zarzycki, K. M. Rosso, Stochastic simulation of isotopic exchange mechanisms for Fe(II)-catalyzed recrystallization of goethite. *Environ. Sci. Technol.* **51**, 7552–7559 (2017).
52. P. Zarzycki, S. Kerisit, K. M. Rosso, Molecular dynamics study of Fe(II) adsorption, electron exchange, and mobility at goethite, (α-FeOOH) Surfaces. *J. Phys. Chem. C* **119**, 3111–3123 (2015).
53. D. E. Latta, C. A. Gorski, M. M. Scherer, Influence of Fe^{2+}-catalysed iron oxide recrystallization on metal cycling. *Biochem. Soc. Trans.* **40**, 1191–1197 (2012).
54. R. M. Handler, B. L. Beard, C. M. Johnson, M. M. Scherer, Atom exchange between aqueous Fe(II) and goethite: An Fe isotope tracer study. *Environ. Sci. Technol.* **43**, 1102–1107 (2009).
55. D. Suter, S. Banwart, W. Stumm, Dissolution of hydrous iron(III) oxides by reductive mechanisms. *Langmuir* **7**, 809–813 (1991).
56. K. H. Nealson, A. R. Rowe, Electromicrobiology: Realities, grand challenges, goals and predictions. *Microb. Biotechnol.* **9**, 595–600 (2016).
57. M. J. Edwards *et al.*, Redox linked flavin sites in extracellular decaheme proteins involved in microbe-mineral electron transfer. *Sci. Rep.* **5**, 11677 (2015).
58. U. Schwertmann, R. M. Cornell, *Iron Oxides in the Laboratory: Preparation and Characterization* (Wiley-VCH, 2000).
59. J. S. LaKind, A. T. Stone, Reductive dissolution of goethite by phenolic reductants. *Geochim. Cosmochim. Acta* **53**, 961–971 (1989).
60. P. Lambrev, Toolbox for analysis of spectroscopy data, version 2.0.0.0. https://www.mathworks.com/matlabcentral/fileexchange/32828-spectr-o-matic/content/peakdet.m. Accessed 1 August 2017.
61. M. L. Fultz, R. A. Durst, Mediator compounds for the electrochemical study of biological redox systems: A compilation. *Anal. Chim. Acta* **140**, 1–18 (1982).
62. C. A. Gorski, L. Klüpfel, A. Voegelin, M. Sander, T. B. Hofstetter, Redox properties of structural Fe in clay minerals. 2. Electrochemical and spectroscopic characterization of electron transfer irreversibility in ferruginous smectite, SWa-1. *Environ. Sci. Technol.* **46**, 9369–9377 (2012).